HHS Public Access

Author manuscript

Neuron. Author manuscript; available in PMC 2020 August 07.

Published in final edited form as:

Neuron. 2019 August 07; 103(3): 423–431.e4. doi:10.1016/j.neuron.2019.05.018.

Paraventricular thalamus projection neurons integrate cortical and hypothalamic signals for cue-reward processing

James M. Otis[1,2,3,4], **ManHua Zhu**[1,4], **Vijay M. K. Namboodiri**[1,2,5], **Cory A. Cook**[1], **Oksana Kosyk**[1], **Ana M. Matan**[1], **Rose Ying**[1], **Yoshiko Hashikawa**[1,5], **Koichi Hashikawa**[1,5], **Ivan Trujillo-Pisanty**[1,5], **Jiami Guo**[2,6,7], **Randall L. Ung**[1], **Jose Rodriguez-Romaguera**[1], **Eva S. Anton**[2,6], **Garret D. Stuber**[1,5,6,8]

[1]Department of Psychiatry, University of North Carolina, Chapel Hill, NC 27599, USA

[2]Neuroscience Center, University of North Carolina, Chapel Hill, NC 27599, USA

[3]Current Address: Department of Neuroscience, Medical University of South Carolina, Charleston, SC 29425, USA

[4]These authors contributed equally to this work.

[5]Current Address: Department of Anesthesiology and Pain Medicine, University of Washington, Seattle, WA 98195, USA

[6]Department of Cell Biology and Physiology, University of North, Chapel Hill, NC 27599, USA

[7]Current Address: Department of Cell Biology & Anatomy University of Calgary, AB Canada

[8]Lead contact.

Summary

The paraventricular thalamus (PVT) is an interface for brain reward circuits, with input signals arising from structures such as prefrontal cortex and hypothalamus that are broadcast to downstream limbic targets. However, the precise synaptic connectivity, activity, and function of PVT circuitry for reward processing are unclear. Here, using *in vivo* two-photon calcium imaging we find that PVT neurons projecting to the nucleus accumbens (PVT-NAc) develop inhibitory responses to reward-predictive cues coding for both cue-reward associative information and behavior. The multiplexed activity in PVTNAc neurons is directed by opposing activity patterns in prefrontal and lateral hypothalamic afferent axons. Further, we find that prefrontal cue encoding may maintain accurate cue-reward processing, as optogenetic disruption of this encoding induced long-lasting effects on downstream PVT-NAc cue responses and behavioral cue discrimination.

Correspondence: gstuber@uw.edu.

Author contributions

JMO, MZ, GDS designed experiments. JMO, MZ, CAC, AMM, OK, RY, YH, KH, IT, JG, JR performed experiments. JMO, MZ, VMKN, RLU analyzed data. JMO, MZ, GDS wrote the paper. GDS supervised the project.

Declaration of Interests

The authors declare no competing interests.

Together, these data reveal that PVT-NAc neurons act as an interface for reward processing by integrating relevant inputs to accurately inform reward-seeking behavior.

eTOC blurb:

The paraventricular nucleus of the thalamus a substrate underlying reward seeking. In this issue of Neuron, Otis, Zhu et al. (2019) demonstrate that projection-defined thalamic neurons are controlled by dissociable response features in cortical and hypothalamic inputs during reward processing.

Introduction

The paraventricular nucleus of the thalamus (PVT) has strong connectivity with brain structures that control reward seeking (Hsu and Price, 2009; Li and Kirouac, 2008), such as the prefrontal cortex (PFC), lateral hypothalamic area (LHA), and nucleus accumbens (NAc). Recent work shows that distinct neurotransmitter inputs to PVT can control separable aspects of reward processing, such as orexinergic control of arousal (Ren et al., 2018), glutamatergic control of cue-reward learning (Otis et al., 2017), and GABAergic control of reward consumption (Zhang and van den Pol, 2017). Thus, it has been suggested that PVT acts as an interface for reward processing, wherein information related to the internal state of an animal and its environmental surroundings are integrated to orchestrate reward-seeking behaviors (Kelley et al., 2005). However, the precise architecture, activity, and function of PVT circuitry for reward processing are largely unknown.

To provide an interface for reward seeking, signals from multiple information streams could converge in PVT to provide a unified output signal. Prelimbic medial PFC glutamatergic neurons and LHA GABAergic neurons may provide such input, as these cells innervate PVT and are critical for cue-reward learning and reward consumption, respectively (Otis et al., 2017; Zhang and van den Pol, 2017). Signals from these input neurons may propagate to several downstream targets, as PVT neurons have bifurcating axon projections throughout the extended amygdala, including the NAc (Dong et al., 2017). In further support of this idea, activity in the PVT-NAc pathway controls arousal (Ren et al., 2018), drug-related behaviors (Zhu et al., 2016), and reward consumption (Do-Monte et al., 2017; Labouèbe et al., 2016; Reed et al., 2018), suggesting that these specific neurons may provide an interface wherein reward-relevant inputs are integrated and broadcast to downstream areas for reward processing. Despite findings showing that PVT and connected circuitry are important for reward seeking, whether PVT-NAc neurons are functionally innervated by PFC and LHA inputs and how each of these circuit elements might be engaged by reward-related stimuli to influence downstream activity and behavior are unknown.

Results

PVT-NAc neurons develop an inhibitory, multiplexed response to reward-predictive cues across learning.

PVT projection neurons have bifurcating axons that innervate several areas of the extended amygdala (Dong et al., 2017; Figure S1), including the NAc that contributes to reward-

seeking behaviors (Koob, 1999). Whether PVT-NAc neurons might encode aspects of reward seeking at the cellular level, however, is unknown. To monitor the activity of PVT-NAc neurons during reward seeking, we used a Pavlovian conditioning task that allowed for two-photon imaging of individual neurons during behavior. Head-fixed mice were trained to associate one conditioned stimulus (CS+), but not another (CS–), with sucrose (Figure 1A and 1B). Following multiple training sessions, mice behaviorally discriminated between the cues by displaying anticipatory licks to the CS+, but not CS− (Figure 1C). To quantify learning, we used an area under the receiver operator characteristic (auROC) curve to compare the probability that licking during the CS+ and CS− trace intervals was equivalent (cue discrimination score ≈ 0), or significantly higher for CS+ versus CS− trials (cue discrimination score > 0). The auROC scores confirmed that mice licked more during the CS+, but only during later behavioral sessions (day 4 or later) and not earlier sessions (Figure 1D). To monitor neuronal activity throughout Pavlovian conditioning, we injected a cre-inducible virus encoding the calcium indicator GCaMP6s (AAVdj-DIO-GCaMP6s; Chen et al., 2013) into the PVT, and in the same surgery injected a retrogradely transported virus encoding cre-recombinase (CAV2-cre; Soudais et al., 2001) into the NAc (Figure 1E). Next, we implanted a microendoscopic lens allowing chronic optical access to PVT-NAc neurons (Figure 1F). Collectively, we recorded from GCaMP6s-expressing PVT-NAc neurons across multiple fields of view (FOVs) early in learning (n=6 mice, 9 FOVs, 312 neurons) and late in learning (n=7 mice, 12 FOVs, 417 neurons). To quantify neuronal cue responses, we used an auROC score to determine whether fluorescence was equivalent (auROC≈0), significantly higher (auROC>0), or significantly lower (auROC<0) during each CS+ or CS− trace interval as compared with corresponding baseline periods. Data revealed that PVT-NAc neurons displayed substantial reductions in their fluorescence in response to a reward-predictive cue late in learning (Figure 1G, 1H, and S2). In contrast, a smaller population of neurons showed increased fluorescence in response to both cues early and late in learning (Figure 1H and S2). To understand how these responses developed, we tracked neuronal responses across learning (Figure 1I and 1J). We found that 52% of tracked neurons displayed a reduction in calcium-mediated fluorescence time-locked to the CS+ across learning, whereas only 14% showed significant increases in fluorescence to the CS+ across learning (Figure 1K). Between these functionally distinct cell populations, CS+ responses were not different early in learning, and CS− responses were also equivalent both early and late in learning (Figure 1L). Thus, the majority of PVT-NAc neurons developed new, inhibitory responses to a reward-predictive cue across learning.

We found that PVT-NAc neurons developed inhibitory cue encoding across learning, during the same time frame wherein mice developed conditioned licking behavior. Thus, we hypothesized that cue responses could represent information related to licking, or could explicitly represent the cue-reward association. To determine how PVT-NAc neuronal cue responses related to licking, using the activity of each PVT-NAc neuron we trained a decoder to predict whether mice licked more or less than average during any given CS+ trial late in learning, as compared with other CS+ trials during the same session. We found that the activity dynamics of single PVT-NAc neurons could be used to predict whether animals licked more or less than their session average as compared with shuffled data from the same animal. In addition, we trained a decoder to predict whether the CS+ had or had not just

been presented during any given trial. We found that the activity dynamics of single PVT-NAc neurons could be used to predict whether the CS+ was delivered late in learning, as compared with shuffled data or data early in learning (Figure 1M and S2). These findings suggest that cue responses in PVT-NAc neurons represent information related to both licking frequency and the cue-reward association.

PFC glutamatergic and LHA GABAergic neurons provide synaptic input to PVT-NAc neurons.

Distinct synaptic inputs could drive independent components of the response observed in PVT-NAc neurons. Two major sources of PVT input arise from prelimbic medial PFC glutamatergic neurons and LHA GABAergic neurons, which respectively contribute to cue-reward learning and feeding (Otis et al., 2017; Zhang and van den Pol, 2017). However, whether PFC and LHA neurons form functional synapses with PVT-NAc neurons is unknown. To evaluate this, a retrogradely-trafficked virus encoding eYFP (retroAAV2-hSyn-eYFP; Tervo et al., 2016) was injected into the NAc, and a virus encoding the red-shifted channelrhodopsin ChrimsonR (ChrR; AAV5-hSyn-ChrR-tdT; Klapoetke et al., 2014) was injected into prelimbic medial PFC. This resulted in ChrR-tdT$^+$ PFC axons surrounding eYFP$^+$ PVT-NAc neurons (Figure 2B). Patch-clamp recordings from PVT-NAc neurons in brain slices revealed that optogenetic activation of PFC axons evoked excitatory (but not inhibitory) postsynaptic currents (EPSCs) in most neurons (79%) that were blocked by the AMPA/kainate glutamate receptor antagonist DNQX (Figure 2 and 2D). In a separate group of animals, the ChrR virus was injected into the LHA, resulting in ChrR-tdT$^+$ LHA axons that were also in close proximity to eYFP$^+$ PVT-NAc neurons (Figure 2E). Patch-clamp recordings from PVT-NAc neurons revealed that optogenetic activation of LHA axons evoked small EPSCs in a subset of cells (35%), but also evoked larger, inhibitory postsynaptic currents (IPSCs) in every recorded cell (100%). These IPSCs were blocked by the $GABA_A$ receptor antagonist GABAzine (Figure 2F and 2G). Thus, PFC axons that are glutamatergic and LHA axons that are primarily GABAergic synaptically innervate PVT-NAc neurons.

PFC and LHA axons that innervate the PVT display distinct response dynamics.

We next targeted PFC and LHA axons within the PVT for *in vivo* two-photon calcium imaging. Previous evidence demonstrated that PFC-PVT glutamatergic neurons and LHA glutamatergic and GABAergic projection neurons express *CaMK2a* (Nieh et al., 2015; Otis et al., 2017). Thus, to visualize activity in PFC or LHA projection neurons, a *CaMK2a* promoter-driven virus encoding GCaMP6s (AAVdj-*CaMK2a*-GCaMP6s) was injected into PFC or LHA, with a lens implanted above PVT (Figure 3A and 3F). The surgery resulted in GCaMP6s expression in PFC or LHA axons (separate groups of mice), that could be visualized in PVT *in vivo* (Figure 3B and 3G). Next, mice underwent Pavlovian conditioning with simultaneous head-fixed two-photon calcium imaging as described above. Data revealed that PFC axons within the PVT primarily display inhibitory responses to the CS+ late in learning, but not early in learning (Figure 3C and 3D). In contrast, LHA axons showed excitatory responses to both cues, with the most robust responses displayed to the CS+ (Figure 3H and 3I). These data suggest that the activity dynamics of both PFC (inhibited, glutamatergic) and LHA (excited, primarily GABAergic) axons could contribute

to inhibitory cue encoding in downstream PVT-NAc neurons. Indeed, decoding analysis revealed that activity in single PFC axons late in learning could be used to more accurately predict whether the CS+ had just been presented, as compared with early in learning or shuffled data. In contrast, the activity of PFC axons could not be used to predict licking frequency (Figure 3E). Interestingly, although activity in single LHA axons could also be used to decode whether or not the CS+ had just been presented as compared with shuffled data, this did not change across learning suggesting that LHA axon responses are related to sensory stimulus detection rather than cue-reward associative information. Furthermore, the activity of LHA axons could be used to predict whether animals were licking more or less than their session average (Figure 3J). Taken together, information related to the cue-reward association is encoded by PFC axons, whereas information related to licking is encoded by LHA axons. PFC and LHA axonal activity may therefore contribute to the multiplexed, inhibitory cue signal found in downstream PVT-NAc neurons.

PFC axon stimulation persistently impairs PVT-NAc cue encoding and behavioral cue discrimination.

Consistent with our results showing lick encoding in the LHA-PVT-NAc pathway, GABA-induced inhibition of the PVT or inhibition of PVT-NAc neurons is known to drive licking and reward consumption (Do-Monte et al., 2017; Stratford and Wirtshafter, 2013; Zhang and van den Pol, 2017). Thus, activity in the LHA-PVT-NAc pathway can contribute to feeding, although the function of cue-reward association encoding in the PFC-PVT-NAc pathway is less clear. Previous studies indicate that PFC cue responses are necessary to maintain and update associative information, such that inhibition of PFC activity during presentation of a reward-predictive cue can persistently reduce behavioral cue responses (Otis et al., 2013). Similarly, PVT cue responses also maintain associative information, as inhibition of these responses can persistently reduce conditioned fear (Do-Monte et al., 2015). Thus, we hypothesized that PFC inputs to PVT-NAc neurons act to maintain cue-reward associative information, such that disruption of PFC axon cue encoding would persistently suppress downstream activity and behavioral cue responses. To determine the function of PFC axonal activity for downstream cue encoding and behavior, a virus encoding ChrR (AAV5-hSyn-ChrR-tdT) was injected into PFC, a virus encoding cre-inducible GCaMP6s (AAVdj-DIO-GCaMP6s) was injected into PVT, and a retrogradely trafficked virus encoding cre-recombinase (CAV2-cre) was injected into the NAc (Figure 4A). This surgery allowed for simultaneous optogenetic activation of PFC axons in PVT during two-photon calcium imaging of downstream PVT-NAc neurons *in vivo* (Figure 4B). Following recovery from surgery, mice underwent Pavlovian conditioning until fully trained, followed by three additional Pavlovian conditioning tests. During the second test mice received optogenetic activation of PFC axons time-locked to each cue presentation, whereas during the first and last tests no optogenetic manipulations were performed (n=3 mice, 5 FOVs). Similar to the previous findings (see Figure 1), PVT-NAc neurons displayed inhibitory responses to the reward-predictive cue during the first test after learning (Figure 4C and 4D, **left panel**). These inhibitory responses were dramatically reversed via optogenetic activation of PFC axons during the second test (Figure 4C and 4D, **middle panel**), and remained significantly attenuated during the third test that took place at least 24 hours after photo-stimulation of PFC-PVT axons (Figure 4C and 4D, **right panel**). In addition, tracked neurons that showed

CS+ responses during the baseline test displayed significant reductions in CS+ responses during the last test (Figure 4E and 4F). Decoding analysis also revealed that activity in PVT-NAc neurons could be used to accurately predict CS+ timing during the first test after learning (similar to previous findings), whereas this prediction accuracy was significantly impaired during the last test after photo-stimulation (Figure 4G). Instead, activity in PVT-NAc neurons could be used to more accurately predict licking frequency during the last test, likely due to the lack of cue-reward association responding that would reduce the reliability of the overall lick decoding. Finally, we found that optogenetic activation of PFC inputs persistently reduced the probability that mice would behaviorally respond to the CS+, and reduced overall behavioral discrimination between the CS+ and CS− (Figure 4H). These long-lasting effects were not simply due to an effect of time (Figure S2), an effect on the ability of mice to lick at high frequencies during the CS+ (Figure 4I), nor an effect of PFC axon activation alone (Figure S4). Taken together, activation of PFC inputs during cue delivery persistently reduced downstream PVT-NAc cue encoding and behavioral cue discrimination.

Discussion

Previously it has been suggested that PVT creates a synaptic interface for reward circuits (Kelley et al., 2005), yet the precise architecture, activity, and function of this circuitry for reward processing are still largely unresolved. Here, we show that PVT-NAc neurons receive monosynaptic input from PFC glutamatergic axons and LHA glutamatergic and GABAergic axons (primarily GABAergic). These inputs drive an inhibitory, multiplexed signal in PVT-NAc neurons, with cue-reward association information relayed by PFC axons and licking information relayed by LHA axons. Although previous evidence reveals that activation of GABAergic inputs can drive reward consumption through PVT-NAc neurons (Do-Monte et al., 2017; Stratford and Wirtshafter, 2013; Zhang and van den Pol, 2017), here we show that activation of a glutamatergic input (from PFC) can persistently suppress behavioral cue discrimination and cue-reward association encoding in PVT-NAc neurons. Together, our data reveal that PVT-NAc neurons create a synaptic interface for reward processing, such that functionally distinct inputs are integrated to accurately guide reward-seeking behavior through downstream circuits.

Our data support the idea that cue encoding in the PFC-PVT-NAc pathway controls and maintains emotionally-relevant associative information. Previously, we found that optogenetic disruption of inhibitory cue encoding in PFC–PVT neurons can prevent cue-reward learning, and can block expression of cue-induced reward seeking without affecting reward seeking in general (Otis et al., 2017). Similarly, optogenetic disruption of excitatory cue responses in PFC–PVT neurons can block cue-evoked fear (Do-Monte et al., 2015), although through a relay to the central amygdala (PFC-PVT-CeA; Do-Monte et al., 2015; Penzo et al., 2015). These data suggest that activity in PFC–PVT neurons can support behavioral responses to salient, emotionally-relevant cues; however, additional data support that PFC–PVT activity can also maintain cue-driven behaviors. For example, systemic or direct inhibition of noradrenergic signaling in PFC can persistently reduce context-driven cocaine seeking in rodents (Fitzgerald et al., 2016; Otis and Mueller, 2011, 2017, Otis et al., 2013, 2014, 2018), recall of emotional words in human subjects (Kroes et al., 2010, 2016),

and recall of heroin-associated words in heroin addicts (Zhao et al., 2010). Furthermore, these effects are associated with long-lasting changes in PFC cue encoding (Kroes et al., 2016) and memory-related synaptic plasticity in PFC projection neurons (Otis and Mueller, 2017). In addition to PFC involvement in maintaining emotionally-relevant associative information, optogenetic inhibition of PVT cue encoding can persistently reduce the expression of cue-conditioned fear, whereas manipulations after cue presentation have no effect (Do-Monte et al., 2015). Thus, considering the long-lasting effects of PFC, PVT, or PFC–PVT manipulations on memory, and the timing-specificity of those effects (during cue exposure, not after), our data support the idea that pre- and post-synaptic coupling in memory circuits during cue delivery is a critical mechanism that maintains memory retrieval. We hypothesize that this activity-dependent maintenance of emotionally-relevant information may allow behavioral flexibility, such that cue-reward or cue-threat associative information is appropriately relayed to downstream targets to accurately guide behavior.

In contrast to inhibitory cue encoding by PFC glutamatergic axons that may underlie memory maintenance, our data support the idea that GABAergic inputs to PVT–NAc neurons can drive feeding. Specifically, PVT infusions of GABA receptor agonists can provoke reward consumption (Stratford and Wirtshafter, 2013), likely through synapses formed by long-range GABAergic inputs (Beas et al., 2018). Neurons in two of these input structures, the LHA and zona incerta (ZI), form a continuum and can both induce feeding through their robust projections to the PVT (Zhang and van den Pol, 2017). Due to the genetic and functional similarities of these inputs, it should be noted that we cannot conclude that effects reported here are completely isolated to LHA-PVT GABAergic neurons. However, because LHA GABAergic cell bodies show similar responses (Jennings et al., 2015) as described in our projection-specific axon recordings, and our histology verifies LHA virus expression, we conclude that our effects are at least predominately mediated through LHA–PVT GABAergic neurons. Regardless, the effects of GABA-mediated inhibition on feeding is likely through PVT–NAc neurons, as these downstream neurons become inhibited in response to rewards (Reed et al., 2018), and such inhibition can drive feeding (Do-Monte et al., 2017; Reed et al., 2018; see also Choudhary et al., 2018). Taken together with findings presented here, long-range GABAergic inputs to PVT–NAc neurons can encode information relevant to rewards and reward consumption, and through this activity provoke feeding.

Multiplexed signals in PVT-NAc neurons not only code for the cue-reward association (PFC glutamatergic inputs) and reward consumption (LHA and other GABAergic inputs) information, but can also provoke a state of arousal and wakefulness through the activity of orexinergic input neurons (a.k.a. hypocretin neurons). During wakefulness, neurons in PVT fire at relatively high frequencies (Kolaj et al., 2012; Novak and Nunez, 1998) to induce a state of arousal and wakefulness (Mátyás et al., 2018; Ren et al., 2018; Zhu et al., 2018), and this high firing rate requires slow, orexin-driven depolarization (Ishibashi et al., 2005). The LHA is the primary source of orexinergic input to PVT, and optogenetic activation of LHA orexinergic input elevates the firing rate of PVT neurons, driving wakefulness through the NAc (Ren et al., 2018). These findings are in striking contrast to the fast, glutamatergic cue encoding or GABAergic lick encoding reported here. Thus, although future studies are required to fully understand the dynamics and function of this pathway, the LHA^{Orexin}-PVT-

NAc circuit may contribute to reward processing by inducing a state of arousal and wakefulness, rather than specifically driving reward seeking or consumption (Martin-Fardon and Weiss, 2014a, 2014b). Considering that orexinergic activity elevates the basal firing rate of PVT–NAc neurons during wakefulness, such findings explain why PFC and LHA inputs could drive rapid reductions in PVT–NAc action potential frequency as reported here. Overall, our data support the idea that PVT–NAc neurons relay an integrated, multiplexed signal coding for arousal/wakefulness (orexin), cue-reward associative information (glutamate), and reward consumption (GABA), such that these diverse stimuli can accurately guide reward-seeking behavior.

Considering the well-established role of the middle-posterior aspect of the PVT for controlling feeding and reward seeking (Bhatnagar and Dallman, 1999; Stratford and Whitford, 2013; Barson et al., 2015), here we focused our experiments on the middle-posterior PVT, rather than anterior PVT. The anterior-posterior gradient of PVT displays distinct connectivity patterns (Li and Kirouac, 2008; 2012), and lesions or inhibition of posterior PVT can facilitate cue-driven reward seeking (Haight et al., 2015; Kuhn et al., 2018) and reward consumption (Bhatnagar and Dallman, 1999; Stratford and Whitford, 2013; Choi and McNally, 2017). Interestingly, inhibition of posterior PVT may only induce reward seeking under certain conditions, such as when there are competing aversive stimuli (Choi and McNally, 2017; see also Do-Monte et al., 2017) or in animals that seek rewards based on goals but not cues (Kuhn et al., 2018). Considering our data, selective experimental effects seen during aversion may be caused by the high firing rate of these neurons under conditions of stress (Beas et al., 2018), causing neuronal inhibition to more robustly modify activity and behavior in those conditions (as seen in Choi and McNally, 2017; Do-Monte et al., 2017). Similarly, since cues reduce the activity of PVT-NAc neurons to unleash reward seeking and consumption (described here, also Do-Monte et al., 2017; Reed et al., 2018), it is understandable that behavioral effects are not seen following further inhibition of this pathway in mice that already use cues to approach rewards (Otis et al., 2017; Kuhn et al., 2018). Thus, to fully investigate the selective role for PVT in reward seeking during conflicting conditions, experiments could be performed wherein PVT output neurons are stimulated rather than inhibited – which may eliminate reward seeking regardless of conflicting circumstances.

STAR METHODS

CONTACT FOR REAGENTS AND RESOURCE SHARING

Information and request for reagents may be directed and will be fulfilled by the corresponding author Garret D. Stuber (gstuber@uw.edu).

EXPERIMENTAL MODEL AND SUBJECT DETAILS

Animals.—C57BL/6J male mice (Jackson Laboratories) aged 8–10 weeks were group housed on a 12-hour reverse light cycle (lights off at 8:00 AM) with littermates until surgery. Behavioral experiments were performed during the dark cycle. All procedures were performed in accordance with the Guide for the Care and Use of Laboratory Animals

(National Institutes of Health), and were approved by the Institutional Animal Care and Use Committee at the University of North Carolina before the experiments began.

METHOD DETAILS

Surgery.—Mice were anesthetized with isoflurane (0.8–1.5%) vaporized in pure oxygen (1–2 liters/minute). Ophthalmic ointment and topical anesthetic (2% Lidocaine; Akorn) were applied, and mice were then placed in a stereotaxic frame. Viruses were administered unilaterally into the middle-posterior region of PVT (300nl; relative to bregma: AP, −1.58mm; ML −1.13mm; DV, −3.30mm; 20° angle), bilaterally into LHA (500nl/side; relative to bregma: AP, −1.3mm; ML −0.9mm; DV, −5.15mm), bilaterally into PFC (500nl/side; relative to bregma: AP, +1.80mm; ML, ±0.60mm; DV, −2.45mm), and/or bilaterally into NAc (500nl/side; relative to bregma: AP, +1.42mm; ML ±0.70mm; DV, −4.80mm). Viruses were packaged by the UNC Vector Core, except for CAV2-cre which was purchased from Institut de Génétique Moléculaire de Montpellier. For two-photon imaging experiments, during the same surgery a chronic indwelling GRIN lens (0.6 mm diameter, 7.3–8.0 mm long; Inscopix, CA) was implanted at a 20° angle dorsolateral to the middle-posterior PVT (relative to bregma: AP, −1.58; ML −1.13mm; DV, −2.95mm), and a custom-made ring (stainless steel; 5mm ID, 11mm OD) was attached to the skull at the same angle to allow subsequent head fixation and two-photon imaging of PVT (see Figure 1A). After surgery, Tylenol was delivered through the drinking water for three days, and mice were allowed to recover with access to both food and water *ad libitum* for 3 weeks or longer. Before Pavlovian conditioning, mice water restricted (water bottles taken out of the cage), and 0.6–1.5 ml of water was delivered every day to a dish placed within each home cage, until mice weighed less than 95% of free drinking weight (~10 days for all experiments). To ensure good health and weight maintenance, mice were weighed and handled daily. This protocol resulted in weight stabilization between 85–95% of free-drinking weight for all mice. No health problems related to dehydration arose at any point from these protocols.

Pavlovian conditioning.—Following surgery and onset of water restriction, mice were habituated to head restraint during which drops of sucrose (12.5% in water; ~3.0 l each) were randomly delivered through a gravity-driven, solenoid-controlled lick spout. Next, mice underwent Pavlovian conditioning wherein two cues (3 kHz pulsing or 12 kHz constant tones, 2 seconds each, 70 dB) were presented 50 times randomly (in a subset of sessions, only 25 cues were presented due to issues with imaging acquisition). After one of the two cues, drops of sucrose were delivered (CS+), whereas no sucrose was delivered after the other cue (CS−). There was a one second pause or ‘trace interval’ between CS+ offset and sucrose delivery, or CS− offset and withholding period. Cue-reward pairings were counterbalanced across mice to ensure that conditioned licking responses occurred for either tone. The inter-trial interval for each cue-reward pairing was chosen as a random sample from a uniform distribution bounded by 20s and 50s. We classified sessions as ‘early in learning’ or ‘late in learning’ based on both behavioral cue discrimination and the day of training. Specifically, sessions were defined as ‘early in learning’ if auROC discrimination scores (see Quantification and Statistical Analysis section) were between −0.35 and +0.35, and the session was on day 4 or earlier. Sessions were defined as ‘late in learning’ if the

animal's auROC discrimination score was greater than +0.40 for at least one session, and if the session was on day 4 or later.

Two-photon microscopy.—A two-photon microscope (Olympus, FVMPE-RS) equipped with the following was used for calcium imaging experiments: a hybrid scanning core with fast resonant scanners for 30Hz frame-rate acquisition, GaAsP-PMT photo detectors with adjustable voltage, gain, and offset features, a single green/red NDD filter cube, a long working distance 20X air objective designed for optical transmission at infrared wavelengths (Olympus, LCPLN20XIR, 0.45NA, 8.3mm WD), a software-controlled modular XY stage loaded on a manual z-deck, and a tunable Mai-Tai Deep See laser system (Spectra Physics, laser set to 955nm, ~100fs pulse width) with automated four-axis alignment. Before each conditioning session, a particular field of view (FOV) was selected by adjusting the imaging plane (z-axis), and each FOV was spaced more than 60 m from one another to prevent visualization of the same cells across multiple FOVs (cell body imaging only, multiple FOVs were not used for axon imaging). Recording sessions were defined as being early in learning or late in learning based on behavioral performance (see 'Pavlovian conditioning').

Optogenetics.—Pulsed visible light delivery through the GRIN lens was coupled with two-photon calcium imaging for full-field stimulation of PFC axonal inputs during recordings of downstream PVT-NAc neurons. To do so, a full-field stimulation kit (FV30SP −LED615, Olympus) was installed onto the same microscope used for other two-photon imaging experiments. Following surgeries wherein PFC axons and PVT−NAc neurons were targeted with ChrR and GCaMP6s, respectively, mice were Pavlovian conditioned. Following conditioning and establishment of 'late in learning' criterion (see 'Pavlovian conditioning'), conditioning continued with each session on a different day. This protocol allowed us to evaluate PVT−NAc cue responses from a particular FOV before, during, and after optogenetic manipulations. Following the baseline session which mimicked normal Pavlovian conditioning, an optogenetic manipulation session was given wherein the LED was presented during the CS+ or CS− periods (5 ms pulses, 20 Hz, 1 mW, 615nm; light was presented for 3 seconds during each tone cue and trace interval). Non-optogenetic Pavlovian conditioning sessions then continued during a following day to determine long-lasting effects of PFC axon activation. In a control experiment, the same procedure occurred except the LED was pulsed randomly outside of the cue-reward pairings. Mice could re-learn the cue-reward association information during the post optogenetic manipulation conditioning session, and thus we limited analysis of behavioral data to the first 25 trials across the 3 test days.

Patch-clamp electrophysiology.—Mice were anesthetized with pentobarbital (50mg/kg) before transcardial perfusion with ice-cold sucrose cutting solution containing the following (in mM): 225 sucrose, 119 NaCl, 1.0 NaH_2PO_4, 4.9 $MgCl_2$, 0.1 $CaCl_2$, 26.2 $NaHCO_3$, 1.25 glucose, ~305 mOsm. Brains were then rapidly removed, and coronal sections 300μm thick were taken while bathed in the cutting solution using a vibratome (Leica, VT 1200). Sections were incubated in aCSF (32°C) containing the following (in mM): 119 NaCl, 2.5 KCl, 1.0 NaH_2PO_4, 1.3 MgCl, 2.5 $CaCl_2$, 26.2 $NaHCO_3$, 15 glucose, ~306 mOsm. After an hour of recovery, slices were constantly perfused with aCSF (32°C)

and visua lized using differential interference contrast through a 40x water-immersion objective mounted on an upright microscope (Olympus BX51WI). Whole-cell recordings were obtained using borosilicate pipettes (3–5 MΩ) back-filled with one of two internal solutions. For current clamp recordings, a potassium gluconate based internal solution composed of the following was used (in mM): 130 K-gluconate, 10 KCl, 10 HEPES, 10 EGTA, 2 $MgCl_2$, 2 ATP, 0.2 GTP (pH 7.35, 270–285 mOsm). For voltage-clamp recordings, a cesium methanesulfonate based internal solution composed of the following was used (in mM): 117 Cs methanesulfonic acid, 20 HEPES, 2.8 NaCl, 5 TEA, 2 ATP, 0.2 GTP, 0.005 MK-801 (pH 7.35, mOsm 280).

Current-clamp recordings were obtained from GCaMP6s-expressing PVT−NAc neurons to identify how action potential frequency correlated with GCaMP6s fluorescence. Specifically, to determine how elevations in action potential frequency influences GCaMP6s fluorescence, a single pulse (0.5−2.0nA, 2ms) was applied to elicit one action potential or the minimum number possible in a burst, since many PVT-NAc neurons fire in bursts rather than through single spikes (see inset of Figure S1E). Similarly, to determine how reductions in action potential frequency influences GCaMP6s fluorescence, a 3 second pause was applied after a 10 second baseline train of depolarizing pulses (0.5−2nA, 2ms; 1Hz). During electrophysiological recordings, GCaMP6s fluorescence dynamics were visualized using a blue LED (490nm; <1mW) integrated into the light path (ThorLabs: catalog #LED4D067), and a microscope-mounted camera (QImaging, optiMOS). Imaging data were acquired using Micro-Manager, and extracted through hand-drawn ROIs for each recorded neuron using ImageJ.

Voltage-clamp recordings were obtained from eYFP-expressing PVT−NAc neurons (visible with the blue LED described above) to identify and characterize monosynaptic inputs from PFC and LHA. During recordings, PVT−NAc neurons were held at −70 and +10 mV for analysis of glutamatergic and GABAergic inputs, respectively. Next, $ChrR^{tdT+}$ axons from PFC or LHA (separate animals for each input) were activated through presentation of a red LED (5 ms pulse; 617 nm; ~1 mW; ThorLabs: catalog #LED4D067) delivered once every 20 to 60 seconds. Cells that showed reliably-reproducible EPSCs in response to light were considered to receive functional, monosynaptic innervation from the activated input structure. In a subset of cells, $GABA_A$ receptors were blocked through bath application of GABAzine (10 μM), whereas AMPA receptors were blocked through bath application of DNQX (10 μM).

Retrograde tracing.—The axonal arborization of PVT projection neurons was evaluated through retrograde tracing. During surgery, the retrograde tracer cholera toxin subunit B conjugated to different Alexa Fluors (CtB−488, CtB−594, CtB−647; Molecular Probes; 0.5% in phosphate buffer) was injected unilaterally into NAc (500nl; relative to bregma: AP, +1.42mm; ML +0.70mm; DV, −4.80mm), BNST (500nl; relative to bregma: AP, +0.14mm; ML +0.60mm; DV, −4.80mm), and CeA (300nl; relative to bregma: AP, −1.34mm; ML +2.32mm; DV, −4.60mm). Ten days following surgery, animals were killed for histology (n=3 mice), and coronal sections containing anterior PVT (−0.58mm from bregma), middle PVT (−1.06mm from bregma), and posterior PVT (−1.58mm from bregma) were taken. Next, a student blind to the experiment and conditions (C.A.C.) counted the number of CtB

−488, CtB−594, and CtB−647 cells in one section for each of the three anterior-posterior regions of PVT. The data were then averaged across these three regions, as no significant differences were found between anterior, middle, and posterior PVT.

QUANTIFICATION AND STATISTICAL ANALYSIS

Calcium imaging data.—Data were both acquired at a 30Hz framerate and processed using a computer equipped with FluoView (Olympus, FV1200) and cellSens (Olympus) software packages. Following data acquisition, videos were motion corrected using a planar hidden Markov model (SIMA; Kaifosh et al., 2014). Datasets that could not be accurately motion corrected were not included in the final analysis (e.g., because of z-motion as this introduces uncorrectable, unrepresentative time-series data). Following motion correction, regions of interest (ROIs) were hand drawn around each dynamic cell or axon segment using the standard deviation projection of the motion-corrected video in ImageJ. Next, calcium transient time series data were extracted from the ROI, and these time-series data were corrected based on the calculated fluorescence of nearby neuropil (Namboodiri et al., *in press*). We found that some visually distinct axon segments had nearly identical waveforms, suggesting that these segments came from the same axon branch or neuron. Thus, all but one of these segments (randomly selected) were excluded for the final analysis to prevent duplication of data. For two-photon imaging experiments that included optogenetics, the optogenetic photo-stimulation led to uncorrectable light artifacts. These light artifacts lasted 5ms, and thus were only a subset of lines from each imaging frame=33ms. Thus, we interpolated these missing data by cutting lines contaminated with the 5ms light pulse for each frame prior to motion correction, and inserting lines from the most recent frame that did not contain a light artifact.

Using the extracted fluorescence datasets, we classified each neuron or axon as an excitatory responder, inhibitory responder, or non-responder. Significant responses represented a significant two-tailed auROC ($p<0.05$) after Benjamini-Hochberg false discovery rate correction, comparing average fluorescence of the CS+ or CS− trace intervals versus a baseline epoch immediately before cue delivery. Each auROC p-value was calculated as that for the corresponding Mann-Whitney U statistic. Chi-squared tests were then used to compare the number of responders across different sessions (e.g., early in learning versus late in learning) and/or across different cues (e.g., CS+ versus CS−). In addition to responder classification, we also classified each tracked neuron as a positive changer, negative changer, or non-changer. To do so, an identical analysis was performed except auROCs represented differences in baseline-subtracted responses (trace interval minus baseline period) between two sessions (e.g., early in learning versus late in learning).

In addition to cell classification, we performed decoding analyses to determine if neuronal activity could be used to predict the timing of cue delivery on any given trial or general licking frequency on any given trial. To do so, we used two identical binary decoders to prevent bias for one variable versus another (as previously described, Otis et al., 2017). In the first, neuronal activity was used to predict whether a cue (CS+ trace interval) or no cue (baseline period) was presented. In the second, neuronal activity was used to predict whether licking frequency during each CS+ trace interval was higher or lower than the mean licking

frequency for all CS+ trace intervals for that particular session. Because in some sessions the variability in conditioned licking rates was very low (generally when the animals were not showing conditioned licking), the binary decoder led to unrepresentative and very high prediction values that were not different from a shuffled control group. We therefore excluded sessions that did not have at least 10 trials with licking rates above the mean, and 10 trials with licking rates below the mean. To complete the decoding analyses, we used the Python module Scikitlearn with GridSearchCV and a support vector classification (SVC) estimator. This included a radial basis function kernel, optimizing across the following parameters: γ: $\{10^{-2}, 10^{-1}, 10^{0}, 10^{1}, 10^{2}\}$, C: $\{10^{-2}, 10^{-1}, 10^{0}, 10^{1}, 10^{2}\}$. Quantification of performance was done using 10-fold validation· For each neuron, the highest accuracy score across these parameters was used as the metric of accuracy. In order to determine whether the population of accuracy scores across all neurons was significantly different from that expected by chance, we performed a single shuffle per neuron by randomizing the cue identity on every trial. The population of shuffled accuracy scores across one shuffle was then compared to the population of unshuffled accuracy scores using a two-tailed Welch's t-test. Note that since the metric of accuracy was optimized across parameters, the mean accuracy score expected by chance is not 0.5, but is instead around 0.55.

Optogenetics.—Licking was quantified during trace intervals for each cue (see Figure 1B), and compared to baseline licking rates using the area under a Receiver Operating Characteristic (auROC; minus 0.5 and then multiplied by 2 such that values could range from −1 to +1). In addition, a cue discrimination auROC was calculated by comparing the number of licks during the CS+ trace interval versus CS− trace interval. Behavioral data were analyzed using a repeated-measures analysis of variance to compare licking performance (auROC scores for each session) between test days. Following a significant effect, Newman-Keuls *post-hoc* tests were used for direct comparison of each test versus the baseline control test.

Electrophysiological data.—Electrophysiological data acquisition occurred at a 10-kHz sampling rate through a MultiClamp 700B amplifier connected to a Digidata 1440A digitizer (Molecular Devices), and were analyzed using Clampfit 10.3 (Molecular Devices).

DATA AND SOFTWARE AVAILABILITY

Python codes written by J.M.O. and V.M.K.N. were used to process and analyze all calcium imaging datasets. These datasets and codes for data analysis are openly available upon request from the corresponding author (gstuber@uw.edu), and the codes used for data processing are openly available online (https://github.com/stuberlab).

Supplementary Material

Refer to Web version on PubMed Central for supplementary material.

Acknowledgements

This study was funded by the National Institutes of Health (F32–DA041184, JMO; R37–DA032750, R01–DA038168, GDS), Brain & Behavior Research Foundation (JMO, GDS, VMKN), Foundation of Hope (GDS),

MUSC Confocal Core (S10 OD021532), UNC Neuroscience Center (Helen Lyng White Fellowship, VMKN), UNC Neuroscience Center Microscopy Core (P30 NS045892), and UNC Department of Psychiatry (GDS).

References

Barson JR, Ho HT, and Leibowitz SF (2015) Anterior thalamic paraventricular nucleus is involved in intermittent access ethanol drinking: role of orexin receptor 2. Addict. Biol 20, 469–481. [PubMed: 24712379]

Beas BS, Wright BJ, Skirzewski M, Leng Y, Hyun JH, Koita O, Ringelberg N, Kwon HB, Buonanno A, and Penzo MA (2018). The locus coeruleus drives disinhibition in the midline thalamus via a dopaminergic mechanism. Nat. Neurosci 21, 963–973. [PubMed: 29915192]

Bhatnagar S, and Dallman MF (1999). The paraventricular nucleus of the thalamus alters rhythms in core temperature and energy balance in a state-dependent manner. Brain Res. 851, 66–75. [PubMed: 10642829]

Chen TW, Wardill TJ, Sun Y, Pulver SR, Renninger SL, Baohan A, Schreiter ER, Kerr RA, Orger MB, Jayaraman V, et al. (2013). Ultrasensitive fluorescent proteins for imaging neuronal activity. Nature 499, 295–300. [PubMed: 23868258]

Choi EA, and McNally GP (2017). Paraventricular thalamus balances danger and reward. J. Neurosi 37, 3018–3029.

Choudhary AG, Somalwar AR, Sagarkar S, Rale A, Sakharkar A, Subhedar NK, Kokare DM (2018). CART neurons in the lateral hypothalamus communicate with the nucleus accumbens shell via glutamatergic neurons in paraventricular thalamic nucleus to modulate reward behavior. Brain Struct. Funct 223, 1313–1328. [PubMed: 29116427]

Do-Monte FH, Quiñones-Laracuente K, and Quirk GJ (2015). A temporal shift in the circuits mediating retrieval of fear memory. Nature 519, 460–463. [PubMed: 25600268]

Do-Monte FH, Minier-Toribio A, Quiñones-Laracuente K, Medina-Colón EM, and Quirk GJ (2017). Thalamic regulation of sucrose seeking during unexpected reward omission. Neuron 94, 388–400. [PubMed: 28426970]

Dong X, Li S, and Kirouac GJ (2017). Collateralization of projections from the paraventricular nucleus of the thalamus to the nucleus accumbens, bed nucleus of the stria terminalis, and central nucleus of the amygdala. Brain Struct. Funct 222, 3927–3943. [PubMed: 28528379]

Fitzgerald MK, Otis JM, and Mueller D (2016). Dissociation of β1- and β2-adrenergic receptor subtypes in the retrieval of cocaine-associated memory. Behav. Brain Res 296, 94–99. [PubMed: 26318933]

Haight JL, Fraser KM, Akil H, and Flagel SB (2015). Lesions of the paraventricular nucleus of the thalamus differentially affect sign- and goal-tracking conditioned responses. Eur. J. Neurosci 42: 2478–2488. [PubMed: 26228683]

Hsu DT, and Price JL (2009). Paraventricular thalamic nucleus: subcortical connections and innervation by serotonin, orexin, and corticotropin-releasing hormone in macaque monkeys. J. Comp. Neurol 512, 825–848. [PubMed: 19085970]

Ishibashi M, Takano S, Yanagida H, Takatsuna M, Nakajima K, Oomura Y, Wayner MJ, and Sasaki K (2005). Effects of orexins/hypocretins on neuronal activity in the paraventricular nucleus of the thalamus in rats in vitro. Peptides 26, 471–481. [PubMed: 15652654]

Jennings JH, Ung RL, Resendez SL, Stamatakis AM, Taylor JG, Huang J, Veleta K, Kantak PA, Aita M, et al. (2015). Visualizing hypothalamic network dynamics for appetitive and consummatory behaviors. Cell 160: 516–527. [PubMed: 25635459]

Kaifosh P, Zaremba JD, Danielson NB, and Losonczy A (2014). SIMA: Python software for analysis of dynamic fluorescence imaging data. Front. Neuroinformatics 8, 80.

Kelley AE, Baldo BA, and Pratt WE (2005). A proposed hypothalamic-thalamic-striatal axis for the integration of energy balance, arousal, and food reward. J. Comp. Neurol 493, 72–85. [PubMed: 16255002]

Kirouac GJ (2015). Placing the paraventricular nucleus of the thalamus within the brain circuits that control behavior. Neurosci. Biobehav. Rev 56, 315–329. [PubMed: 26255593]

Klapoetke NC, Murata Y, Kim SS, Pulver SR, Birdsey-Benson A, Cho YK, Morimoto TK, Chuong AS, Carpenter EJ, Tian Z, et al. (2014). Independent optical excitation of distinct neural populations. Nat. Methods 11, 338–346. [PubMed: 24509633]

Kolaj M, Zhang L, Rønnekleiv OK, and Renaud LP (2012). Midline thalamic paraventricular nucleus neurons display diurnal variation in resting membrane potentials, conductances, and firing patterns in vitro. J. Neurophysiol 107, 1835–1844. [PubMed: 22219029]

Koob GF (1999). The role of the striatopallidal and extended amygdala systems in drug addiction. Ann. N. Y. Acad. Sci 877, 445–460. [PubMed: 10415664]

Kroes MCW, Strange BA, and Dolan RJ (2010). Beta-adrenergic blockade during memory retrieval in humans evokes a sustained reduction of declarative emotional memory enhancement. J. Neurosci 30, 3959–3963. [PubMed: 20237266]

Kroes MCW, Tona KD, den Ouden HEM, Vogel S, van Wingen GA, and Fernández G (2016). How administration of the beta-blocker propranolol before extinction can prevent the return of fear. Neuropsychopharmacology 41, 1569–1578. [PubMed: 26462618]

Kuhn BN, Klumpner MS, Covelo IR, Campus P, and Flagel SB (2018). Transient inactivation of the paraventricular nucleus of the thalamus enhances cue-induced reinstatement in goal-trackers, but not sign-trackers. Psychopharmacology 235, 999–1014. [PubMed: 29285634]

Labouèbe G, Boutrel B, Tarussio D, and Thorens B (2016). Glucose-responsive neurons of the paraventricular thalamus control sucrose-seeking behavior. Nat. Neurosci 19, 999–1002. [PubMed: 27322418]

Li S, and Kirouac GJ (2008). Projections from the paraventricular nucleus of the thalamus to the forebrain, with special emphasis on the extended amygdala. J. Comp. Neurol 506, 263–87. [PubMed: 18022956]

Li S, and Kirouac GJ (2012). Sources of inputs to the anterior and posterior aspects of the paraventricular nucleus of the thalamus. J. Comp. Neurol 217, 257–273.

Martin-Fardon R, and Weiss F (2014a). Blockade of hypocretin receptor-1 preferentially prevents cocaine seeking: comparison with natural reward seeking. Neuroreport 25, 485–488. [PubMed: 24407199]

Martin-Fardon R, and Weiss F (2014b). N-(2-methyl-6-benzoxazolyl)-N'−1,5-naphthyridin-4-yl urea (SB334867), a hypocretin receptor-1 antagonist, preferentially prevents ethanol seeking: comparison with natural reward seeking. Addict. Biol 19, 233–236. [PubMed: 22830647]

Mátyás F, Komlósi G, Babiczky Á, Kocsis K, Barthó P, Barsy B, Dávid C, Kanti V, Porrero C, Magyar A, et al. (2018). A highly collateralized thalamic cell type with arousal-predicting activity serves as a key hub for graded state transitions in the forebrain. Nat. Neurosci 21, 1551–1562. [PubMed: 30349105]

Namboodiri VMK, Otis JM, van Heeswijk K, Voets ES, Alghorazi RA, Rodriguez-Romaguera J, Mihalas S, and Stuber GD (in press) Single-cell activity tracking reveals that orbitofrontal neurons acquire and maintain a long-term memory to guide behavioral adaptation. Nat. Neurosci

Nieh EH, Matthews GA, Allsop SA, Presbrey KN, Leppla CA, Wichmann R, Neve R, Wildes CP, and Tye KM (2015). Decoding neural circuits that control compulsive sucrose seeking. Cell 160, 528–541. [PubMed: 25635460]

Novak CM, and Nunez AA (1998). Daily rhythms in Fos activity in the rat ventrolateral preoptic area and midline thalamic nuclei. Am. J. Physiol 275, R1620–1626. [PubMed: 9791082]

Otis JM, and Mueller D (2011). Inhibition of β-adrenergic receptors induces a persistent deficit in retrieval of a cocaine-associated memory providing protection against reinstatement. Neuropsychopharmacology 36, 1912–1920. [PubMed: 21544069]

Otis JM, and Mueller D (2017). Reversal of cocaine-associated synaptic plasticity in medial prefrontal cortex parallels elimination of memory retrieval. Neuropsychopharmacology 42, 2000–2010. [PubMed: 28466871]

Otis JM, Dashew KB, and Mueller D (2013). Neurobiological dissociation of retrieval and reconsolidation of cocaine-associated memory. J. Neurosci 33, 1271–1281a. [PubMed: 23325262]

Otis JM, Fitzgerald MK, and Mueller D (2014). Inhibition of hippocampal β-adrenergic receptors impairs retrieval but not reconsolidation of cocaine-associated memory and prevents subsequent reinstatement. Neuropsychopharmacology 39, 303–310. [PubMed: 23907403]

Otis JM, Namboodiri VMK, Matan AM, Voets ES, Mohorn EP, Kosyk O, McHenry JA, Robinson JE, Resendez SL, Rossi MA, et al. (2017). Prefrontal cortex output circuits guide reward seeking through divergent cue encoding. Nature 543, 103–107. [PubMed: 28225752]

Otis JM, Fitzgerald MK, Yousuf H, Burkard JL, Drake M, and Mueller D (2018). Prefrontal neuronal excitability maintains cocaine-associated memory during retrieval. Front. Behav. Neurosci 12, 119. [PubMed: 29962941]

Penzo MA, Robert V, Tucciarone J, De Bundel D, Wang M, Van Aelst L, Darvas M, Parada LF, Palmiter RD, He M, et al. (2015). The paraventricular thalamus controls a central amygdala fear circuit. Nature 519, 455–459. [PubMed: 25600269]

Reed SJ, Lafferty CK, Mendoza JA, Yang AK, Davidson TJ, Grosenick L, Deisseroth K, and Britt JP (2018). Coordinated reductions in excitatory input to the nucleus accumbens underlie food consumption. Neuron 99, 1260–1273. [PubMed: 30146308]

Ren S, Wang Y, Yue F, Cheng X, Dang R, Qiao Q, Sun X, Li X, Jiang Q, Yao J, et al. (2018). The paraventricular thalamus is a critical thalamic area for wakefulness. Science 362, 429–434. [PubMed: 30361367]

Soudais C, Laplace-Builhe C, Kissa K and Kremer EJ (2001). Preferential transduction of neurons by canine adenovirus vectors and their efficient retrograde transport in vivo. FASEB J. 15, 2283–2285 (2001). [PubMed: 11511531]

Stratford TR, and Wirtshafter D (2013). Injections of muscimol into the paraventricular thalamic nucleus, but not mediodorsal thalamic nuclei, induce feeding in rats. Brain Res. 1490, 128–133. [PubMed: 23111346]

Tervo DGR, Hwang BY, Viswanathan S, Gaj T, Lavzin M, Ritola KD, Lindo S, Michael S, Kuleshova E, Ojala D, et al. (2016). A designer AAV variant permits efficient retrograde access to projection neurons. Neuron 92, 372–382. [PubMed: 27720486]

Vertes RP, and Hoover WB (2008). Projections of the paraventricular and paratenial nuclei of the dorsal midline thalamus in the rat. J. Comp. Neurol 508, 212–237. [PubMed: 18311787]

Zhang X, and van den Pol AN (2017). Rapid binge-like eating and body weight gain driven by zona incerta GABA neuron activation. Science 356, 853–859. [PubMed: 28546212]

Zhao LY, Shi J, Zhang XL, Epstein DH, Zhang XY, Liu Y, Kosten TR, and Lu L (2010). Stress enhances retrieval of drug-related memories in abstinent heroin addicts. Neuropsychopharmacology. 35, 720–726. [PubMed: 19890257]

Zhu Y, Wienecke CFR, Nachtrab G, and Chen X (2016). A thalamic input to the nucleus accumbens mediates opiate dependence. Nature 530, 219–222. [PubMed: 26840481]

Zhu Y, Nachtrab G, Keyes PC, Allen WE, Luo L, and Chen X (2018). Dynamic salience processing in paraventricular thalamus gates associative learning. Science 362, 423–429. [PubMed: 30361366]

Highlights:

- PVT-NAc neurons develop inhibitory response to reward-predictive cues.
- Glutamatergic PFC axons to PVT show reductions in activity to cues.
- GABAergic LHA axons to PVT show increases in their activity during licking.
- Optogenetic stimulation of PFC axons disrupts PVT-NAc cue encoding and behavior.

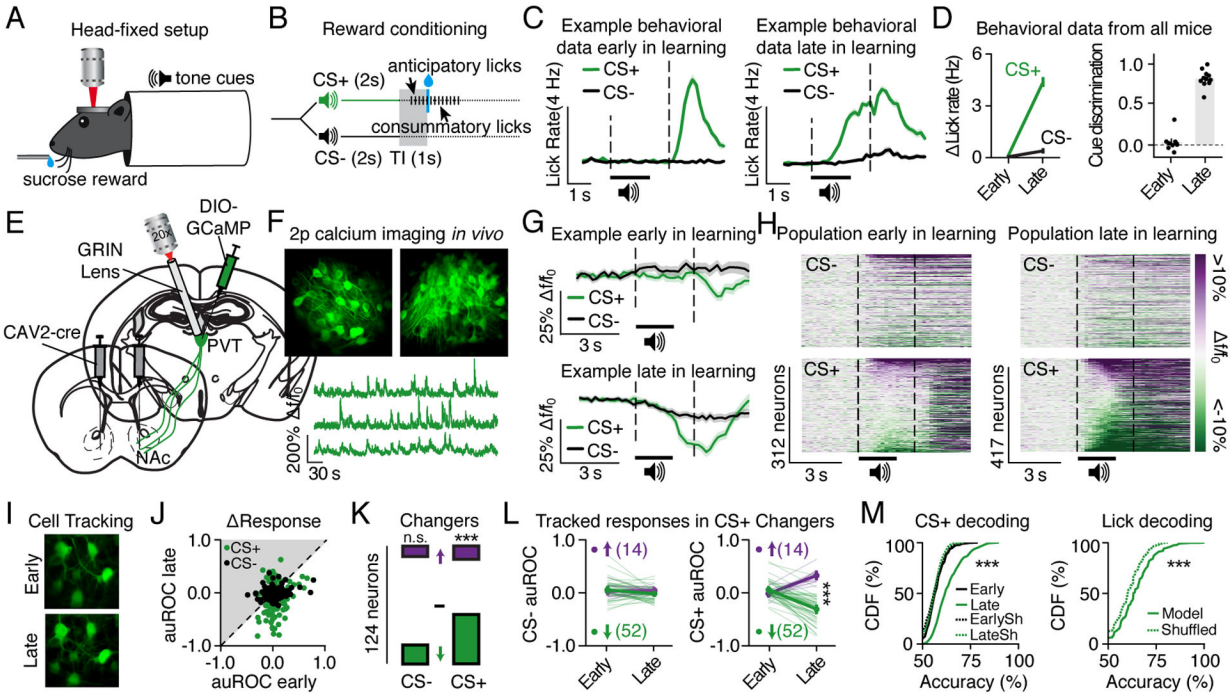

Figure 1. PVT-NAc neurons develop an inhibitory, multiplexed response to reward-predictive cues across learning.

(A–B) Schematics showing head fixation for two-photon imaging experiments (A) and design of Pavlovian conditioning procedures (B; TI, trace interval).

(C) Example data showing averaged licking frequency during the CS+ and CS− for a single mouse early (left) and late (right) in learning.

(D) Grouped data showing lick rates during the CS+ versus CS− (left). Higher cue discrimination scores (right) during sessions late in learning (n=7 mice, 12 sessions) versus sessions early in learning (n=6 mice, 9 sessions; t_{19}=16.7, p<0.001). Data are mean ± standard error.

(E-F) Viral strategy (E) allowed recordings of GCaMP6s-expressing PVT-NAc neurons (early, 9 FOVs, n=312 neurons; late, 12 FOVs, n=417 neurons) *in vivo* (F).

(G-H) Fluorescent traces from a tracked example neuron (G) and heat plots from all neurons (H) showing cue responses in sessions early and late in learning.

(I) Representative images showing PVT-NAc cells tracked across learning.

(J) Neuronal cue responses from cells tracked across learning (n=5 mice, 7 FOVs, 124 neurons).

(K) Quantification of tracked responses showing the proportion of cells that showed increased activity (purple), no change (white) or reduced activity (green) in response to the CS− or CS+ during a session late in learning versus a session early in learning (corrected auROC p-value<0.05 for significant ‘changers’). More cells developed reduced activity (versus cells showing increased activity) during the CS+ across learning ($\chi^{2=}$17.7, p<0.001). An equivalent number of cells developed reduced activity (versus cells showing increased activity) during the CS− across learning (χ^2=2.1, p=0.15).

(L) Tracked cue responses in CS+ changers only (n=52 reducers; 14 increasers), revealing that CS+ but not CS− responses were displayed late in learning, whereas no differences were

displayed early in learning (CS+, 2-way ANOVA: Interaction $F_{1,64}$=152.0, p<0.001; CS-, 2-way ANOVA: $F_{1,64}$=2.3, p=0.14; *** indicates post-hoc p<0.001). Data are mean ± standard error.

(M) Cumulative distribution frequency (CDF) plots showing the dynamics of individual PVT-NAc neurons could be used to predict the timing of the CS+ late in learning (left, versus early in learning: Welch's $t_{711.8}$=13.8, p<0.001) and could also be used to predict licking frequency (right, versus shuffled: Welch's $t_{809.1}$=6.5, p<0.001). EarlySh, shuffled data from sessions early in learning; LateSh, shuffled data from sessions late in learning. See also Figures S1, S2, and S3.

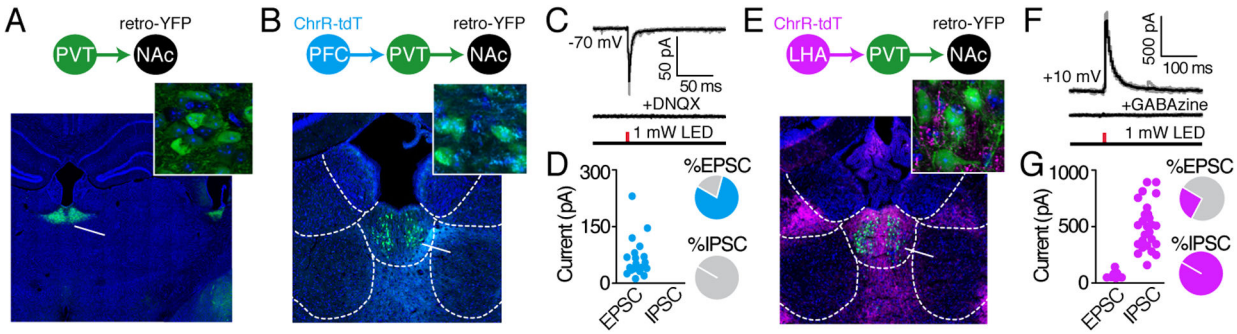

Figure 2. PFC glutamatergic and LHA GABAergic neurons provide synaptic input to PVT NAc neurons.

(A–B) Labeling of PVT-NAc neurons (A) and PFC axons resulted in co-localization of PVT–NAc^{eYFP+} neurons and PFC^{tdT+} axons (B). Scale bars are 500μm (A, main image), 250μm (B, main image), and 25μm (insets).

(C) Representative EPSCs evoked by optogenetic stimulation of PFC axons during patch-clamp recordings (n=4 mice, 24 neurons).

(D) Grouped data showing that 79% of recorded PVT-NAc neurons displayed EPSCs in response to optogenetic stimulation of PFC axons, whereas 0% showed IPSCs.

(E) Labeling of PVT-NAc neurons and LHA axons resulted in co-localization of PVT-NAc^{eYFP+} neurons and LHA^{tdT+} axons. Scale bars are 250μm (main image) and 25μm (inset).

(F) Representative IPSCs evoked by optogenetic stimulation of LHA axons during patch-clamp recordings (n=2 mice, 26 neurons).

(G) Grouped data showing that 100% of recorded PVT-NAc neurons displayed IPSCs in response to optogenetic stimulation of LHA axons, whereas only 35% showed EPSCs.

See also Figure S3.

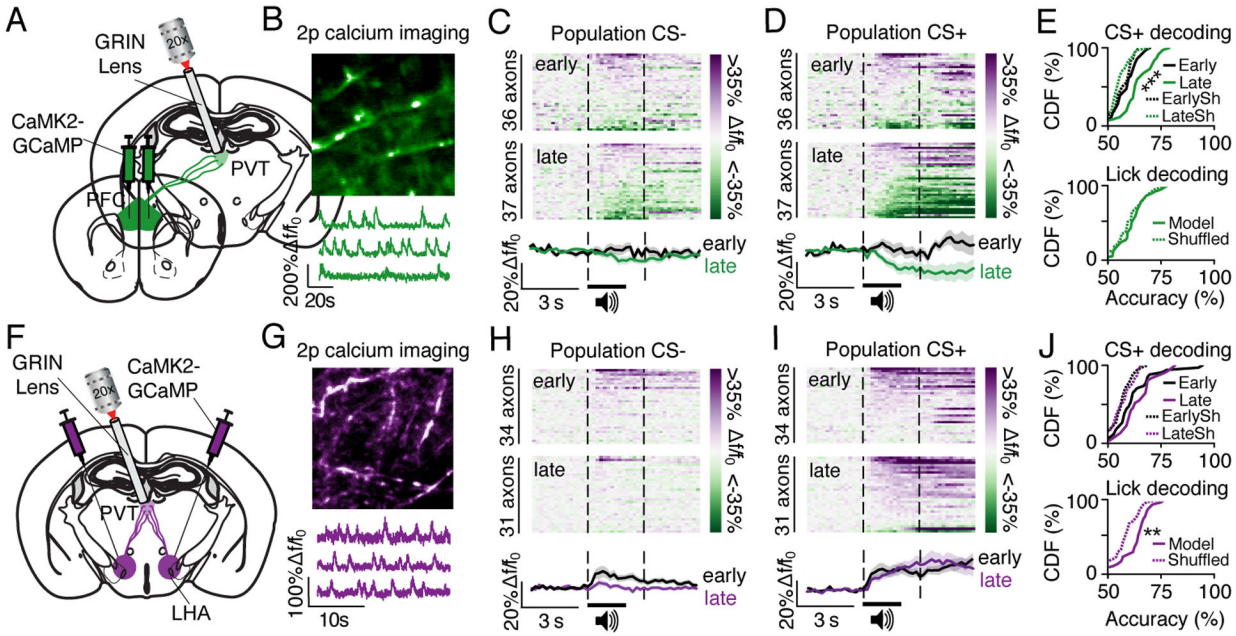

Figure 3. PFC and LHA axons that innervate the PVT display distinct response dynamics.

(A-B) Viral strategy (A) allowed recordings of GCaMP6s-expressing PFC axons (see arrows; early learning, n=4 mice, 4 FOVs, 36 axons; late learning, n=4 mice, 4 FOVs, 37 axons) *in vivo* (B).

(C-D) Population heat plots showing averaged CS− responses (C) and CS+ responses (D) for each PFC axon in sessions early in learning (top) and late in learning (middle). Fluorescent traces show cue responses averaged across all neurons (bottom).

(E) Cumulative distribution frequency (CDF) plots showing that the dynamics of individual PFC axons could be used to more accurately predict the timing of the CS+ late in learning versus early in learning (top, Welch's $t_{67.4}$=3.8, p<0.001), but could not be used to accurately predict licking frequency (bottom, versus shuffled: Welch's $t_{71.6}$=0.9, p=0.35). EarlySh, shuffled data from sessions early in learning; LateSh, shuffled data from sessions late in learning.

(F-G) Viral strategy (F) allowed recordings of GCaMP6s-expressing LHA axons (see arrows; early, n=4 mice, 4 FOVs, 34 axons; late, n=4 mice, 4 FOVs, n=31 axons) *in vivo* (G).

(H-I) Population heat plots showing averaged CS-responses (H) and CS+ responses (I) for each LHA axon in sessions early in learning (top) and late in learning (middle). Fluorescent traces show cue responses averaged across all neurons (bottom).

(J) Cumulative distribution frequency (CDF) plots showing that the dynamics of individual LHA axons could not be used to accurately predict the timing of the CS+ late in learning (top, versus CS+ predictions early in learning: Welch's $t_{61.2}$=0.92, p=0.36), but could be used to accurately predict licking frequency (bottom, versus shuffled: Welch's $t_{59.2}$=2.5, p=0.01). EarlySh, shuffled data from sessions early in learning; LateSh, shuffled data from sessions late in learning.

See also Figure S3.

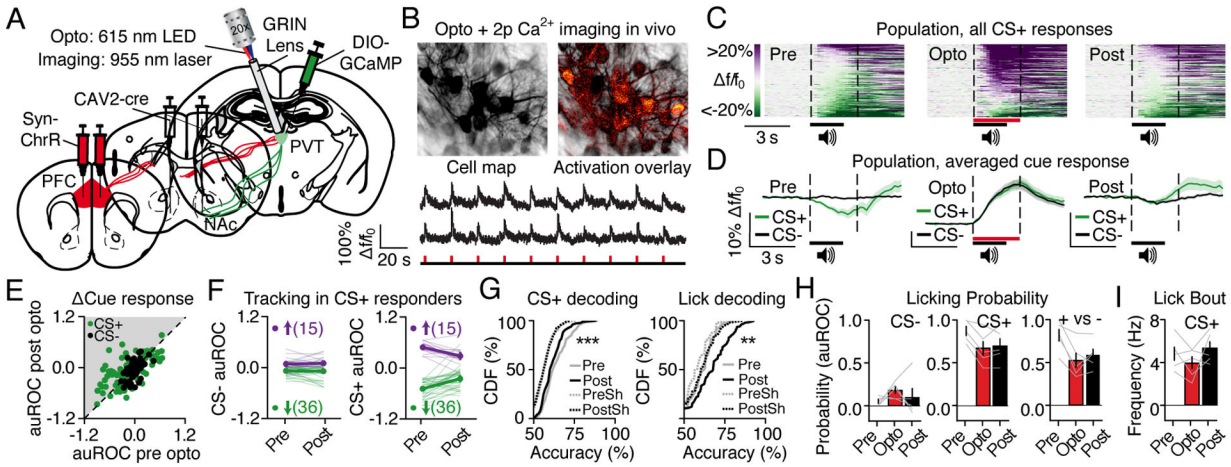

Figure 4. PFC axon stimulation persistently impairs PVT-NAc cue encoding and behavioral cue discrimination.

(A) Viral strategy for optogenetic excitation of PFC axons during two-photon calcium imaging of PVT-NAc neurons.

(B) Cell map, activation overlay (top; red pixels are those with increased fluorescence during activation of PFC axons), and representative traces (bottom) showing optogenetic activation of PFC axons reliably induced excitatory fluorescent deflections in PVT-NAc neurons (n=3 mice, 5 FOVs).

(C) Population heat plot from all PVT-NAc neurons showing averaged CS+ responses during the Pre-Opto session (n=197 neurons), Opto session (n=165 neurons), and Post-Opto session (n=184 neurons).

(D) Fluorescence traces showing CS+ and CS− responses averaged across all PVT-NAc neurons.

(E) Neuronal CS+ and CS− responses from all cells tracked from the Pre-Opto session to Post-Opto session (n=95 neurons).

(F) Tracked cue responses in Pre-Opto CS+ responding neurons (n=36 inhibited, 15 excited). Data show CS+ responses were attenuated during the Post-Opto session in inhibited neurons (t_{35}=−4.7, p<0.001) and in excited neurons (t_{14}=4.2, p<0.001), whereas CS− responses were unchanged (inhibited neurons, t_{35}=0.3, p=0.7; excited neurons, t_{14}=0.5, p=0.7). Data are mean ± standard error.

(G) Cumulative distribution frequency (CDF) plots showing that the activity of PVT-NAc neurons more accurately predicted CS+ timing during the Pre-Opto versus Post-Opto session (left, Welch's $t_{376.6}$=3.2, p=0.001). Activity more accurately predicted licking frequency during the Post-Opto session (right, Welch's $t_{254.9}$=3.0, p=0.003). PreSh, shuffled data from sessions before optogenetic stimulation; PostSh, shuffled data from sessions after optogenetic stimulation.

(H) Grouped behavioral data revealing equivalent lick probability during the CS− for all sessions (left, ANOVA: $F_{2,8}$=1.0, p=0.4; n=5). Lick probability was less during the CS+ for the Opto and Post-Opto sessions, versus the Pre-Opto session (middle, ANOVA: $F_{2,8}$=14.5, p=0.002; n=5). Cue discrimination scores were lower during the Opto and Post-Opto sessions, as compared to the Pre-Opto session (right, ANOVA: $F_{2,8}$=11.2, p=0.005; n=5; **indicates Newman Keuls post-hoc p<0.01). Data are mean ± standard error.

(I) Grouped behavioral data revealing that in trials wherein mice licked during the CS+, the lick bout frequency was equivalent across sessions (ANOVA: $F_{2,8=}1.6$, p=0.3; n=5). Data are mean ± standard error.

See also Figure S3 and S4.

KEY RESOURCES TABLE

REAGENT or RESOURCE	SOURCE	IDENTIFIER
Chemicals, Peptides, and Recombinant Proteins		
DNQX (6,7-Dinitroquinoxaline-2,3(1H,4H)-dione)	Sigma-Aldrich	Cat. No. 2379-57-9
GABAzine (SR 95531 hydrobromide)	Tocris Bioscience	Cat. No. 1262
Experimental Models: Organisms/Strains		
C57BL/6J mice	Jackson Laboratory	N/A
Recombinant DNA		
AAVdj-CaMKIIa-GCaMP6s	UNC Vector Core	AAV Custom Prep
AAVdj-EF1a-DIO-GCaMP6s	UNC Vector Core	AAV Custom Prep
AAV5-hSyn-ChrimsonR-tdTomato	UNC Vector Core	Boyden Vector
CAV2-cre (CMV promoter, SV40 poly(A) tail)	Institut de Génétique Moléculaire de Montpellier	CAV-2 Cre
Software and Algorithms		
Calcium imaging data analysis scripts (Python)	This Paper	github.com/stuberlab
ImageJ	Schneider et al., 2012	imagej.nih.gov/ij/
MATLAB	Mathworks	mathworks.com
Prism 7	GraphPad	graphpad.com
Python	Anaconda	conda.io
SIMA v1.3	Kaifosh et al., 2014	github.com/losonczylab/sima